Timing of CFTR pore opening and structure of its transition state

Ben Sorum[1,2], Dávid Czégé[2], and László Csanády[1,2*]

Character count: 53777

[1]Department of Medical Biochemistry and [2]MTA-SE Ion Channel Research Group, Semmelweis University, Tűzoltó u. 37-47, Budapest, H-1094, Hungary

*Correspondance:

László Csanády

E-mail: csanady.laszlo@med.semmelweis-univ.hu

Summary

In CFTR, the chloride ion channel mutated in cystic fibrosis (CF) patients, pore opening is coupled to ATP binding-induced dimerization of two cytosolic nucleotide binding domains (NBDs), and closure to dimer disruption following ATP hydrolysis. CFTR opening rate, unusually slow because of its high-energy transition state, is further slowed by CF mutation ΔF508. Here we exploit equilibrium gating of hydrolysis-deficient CFTR mutant D1370N, and apply Rate-Equilibrium Free Energy Relationship analysis to estimate relative timing of opening movements in distinct protein regions. We find clear directionality of motion along the longitudinal protein axis, and identify an opening transition-state structure with the NBD dimer formed but the pore still closed. Thus, strain at the NBD/pore-domain interface, the ΔF508 mutation locus, underlies the energetic barrier for opening. Our findings suggest a therapeutic opportunity to stabilize this transition-state structure pharmacologically in ΔF508-CFTR to correct its opening defect, an essential step towards restoring CFTR function.

Introduction

The Cystic Fibrosis (CF) Transmembrane Conductance Regulator (CFTR) is the chloride ion channel mutated in patients suffering from CF, a devastating multiorgan disease (O'Sullivan and Freedman, 2009). The majority (~90%) of CF patients carry at least one allele with a deletion of phenylalanine 508 (ΔF508). The ΔF508 mutation severely impairs both surface expression (Cheng et al., 1990) and chloride channel function (Miki et al., 2010) of CFTR. Even if efforts to promote trafficking to the surface prove successful, understanding the molecular mechanism of the functional defect in ΔF508 CFTR will still be essential for its correction in CF patients.

CFTR belongs to the family of ATP Binding Cassette (ABC) transporters (Riordan et al., 1989), which are built from two homologous halves, each comprising a transmembrane domain (TMD; Fig. 1A-B, *gray*) followed by a cytosolic nucleotide binding domain (NBD; Fig. 1A-B, *green* and *blue*). In CFTR these two halves (TMD1-NBD1 and TMD2-NBD2) are linked by the unique cytosolic regulatory (R) domain (Fig. 1A, *top*, *magenta*), a target for phosphorylation by cAMP-dependent protein kinase (PKA) (Riordan et al., 1989); R-domain phosphorylation is a prerequisite for CFTR chloride channel activity (Tabcharani et al., 1991).

Opening and closing (gating) of the CFTR chloride ion pore, formed by its TMDs, is coupled to a conserved ATP binding/hydrolysis cycle at the NBDs (Fig. 1B). In ABC proteins ATP binding triggers association of the two NBDs into a stable head-to-tail dimer which occludes two molecules of ATP (Fig. 1B, *yellow circles*) at the interface (e.g., (Smith et al., 2002)). By forming strong interactions with conserved residues of both the Walker motifs in the head of one NBD and the signature sequence in the tail of the opposing NBD these ATP molecules act as molecular glue which ties the NBDs together: prompt dimer disruption therefore requires ATP hydrolysis (Moody et al., 2002). In CFTR only the composite binding site formed by Walker A and B motifs of NBD2 and the signature sequence of NBD1 (site 2; Fig. 1B, *upper site*) is catalytically active; the other interfacial binding site (site 1; Fig. 1B, *lower site*) is degenerate and keeps ATP bound and unhydrolyzed throughout several NBD dimerization cycles (Aleksandrov et al., 2002; Basso et al., 2003). In ABC exporters NBD dimer formation flips the TMDs to an outward-facing orientation, while dimer disruption following ATP hydrolysis and substrate release resets them to inward-facing; NBD-to-TMD signal transmission is

mediated by an interface which includes four short "coupling helices" (CH1-4) (Locher, 2009) in TMD intracellular loops (Fig. 1A, *violet loops*). In CFTR NBD dimer formation initiates a burst of pore openings interrupted by brief closures, while dimer dissociation terminates the burst and returns the TMDs into a long-lasting nonconducting (interburst) state (Vergani et al., 2005). Functional studies confirm that in the bursting ("open") state CFTR's TMDs resemble the outward-, whereas in the interburst ("closed") state they resemble the inward-facing conformation of ABC exporter TMDs (Bai et al., 2011; Cui et al., 2014; Wang et al., 2014a). For wild-type (WT) CFTR gating is a unidirectional cycle: most openings are terminated by ATP hydrolysis (Fig. 1B; step $O_1 \rightarrow O_2$) rather than by far slower non-hydrolytic closure (Fig. 1B; step $O_1 \rightarrow C_1$; rate k_{OC}) (Csanády et al., 2010).

The major functional defect of ΔF508 CFTR is a >40-fold reduction in opening rate (Miki et al., 2010; Kopeikin et al., 2014), which reflects destabilization – relative to the closed state – of the transition state for channel opening (step $C_1 \rightarrow O_1$; Fig. 1B; rate k_{CO}). Insight into the dynamics of this opening conformational change and the structure of its transition state would be a key step forward in understanding the molecular mechanism of the ΔF508 gating defect.

Transition states, which determine the rates of functionally relevant conformational movements, are the highest-energy, shortest-lived conformations of proteins. For instance, for ion channels closed↔open conformational transitions are so fast that they appear as single steps even in the highest time-resolution recordings, implying that the time the channel protein spends in the transition state itself is on the sub-microsecond scale – in contrast to the long (milliseconds-seconds) intervals spent in comparatively stable open and closed ground states observable in single-channel recordings (Figs. 2A-5A). Intractable by standard structural biological approaches, transition-state structures can be studied using Rate-Equilibrium Free Energy Relationship (REFER) analysis, which reports on the relative timing of movements in selected protein regions during a conformational transition, such as a channel opening step (Zhou et al., 2005; Auerbach, 2007). Structural perturbations (typically point mutations) in a given channel region often change channel open probability (P_o) by affecting the open-closed free energy difference, but the extent to which the free energy of the *barrier* that must be traversed in opening or closing the channel is affected depends on how early or late that region moves. A region that moves early during opening will have already approached its open-state conformation in the

overall transition state: a perturbation here thus affects the stability of the transition state to an extent similar to that of the open state, and so impacts only opening, but not closing, rate. In contrast, a region that moves late during opening is still near its closed-state conformation in the transition state: a perturbation here that affects open-state stability thus does not affect transition-state stability and so impacts only closing, but not opening, rate. This relative timing of motion of a given region of the channel protein is reported by its Φ value, the slope of a log-log plot of opening rate (k_{CO}) versus equilibrium constant ($K_{eq}=P_o/(1-P_o)$) for a series of structural perturbations (Brønsted plot): a large Φ value (close to 1) indicates early, and a small Φ value (close to 0) late, movement.

REFER analysis has been extremely fruitful in mapping gating dynamics of the nicotinic acetylcholine receptor channel (e.g., (Mitra et al., 2005; Purohit et al., 2007; Purohit et al., 2013; Purohit et al., 2015)), but is applicable only to equilibrium mechanisms (Csanády, 2009), unlike that of CFTR. This drawback has so far hampered insight into the CFTR opening transition state. Here we exploit a catalytic site mutation which abolishes ATP hydrolysis and so truncates the CFTR gating cycle to an equilibrium process. In this non-hydrolytic background we employ the REFER technique to address the relative timing of movements within the sub-microsecond process of pore opening in three spatially distant positions distributed along the longitudinal axis (cytoplasmic to extracellular) of the CFTR protein. Our results identify a conformation-change wave with clear directionality, and provide direct measurements that outline the global structure of the CFTR opening transition state.

Results

Choice of a background construct suitable for REFER studies

ATP hydrolysis in ABC proteins is destroyed by mutations of the Walker B aspartate (Urbatsch et al., 1998; Hrycyna et al., 1999; Rai et al., 2006) which coordinates Mg^{2+} at each active site (Hung et al., 1998; Hopfner et al., 2000). To make CFTR gate at equilibrium, we introduced the NBD2 Walker-B mutation D1370N (Fig. 1A, *bottom*, *red star*) because, among several hydrolysis-disrupting mutations tested, D1370N only slightly reduces the apparent affinity for ATP, and does not prolong open bursts to an extent incompatible with single-channel gating analysis (Csanády et al., 2010).

PKA- and ATP-dependent regulation of CFTR gating are intertwined, and the mechanism of R-domain action is poorly understood: evidence exists for its direct interaction with both NBDs and TMDs (Wang et al., 2002; Bozoky et al., 2013). Thus, changes in gating kinetics caused by perturbations of a target position might potentially reflect altered R-domain/target position interactions, rather than energetic effects on ATP-dependent conformational transitions. Such confounding effects are absent in channels lacking the R domain: cut-ΔR channels, obtained by coexpression of TMD1-NBD1 (residues 1-633) and TMD2-NBD2 (residues 837-1480), do not require phosphorylation to be active, while ATP-dependent gating remains similar to WT (Csanády et al., 2000).

Thus, we chose cut-ΔR(D1370N) as the background construct for our REFER study (Fig. 1A, *bottom*). Gating of cut-ΔR(D1370N) indeed proved PKA-independent, but remained strictly ATP-dependent with an apparent affinity for ATP of 288±27 μM (Fig. S1A-B). Just as for WT (Winter et al., 1994; Zeltwanger et al., 1999; Csanády et al., 2000; Vergani et al., 2003), cut-ΔR (Csanády et al., 2000; Bompadre et al., 2005), and D1370N (Vergani et al., 2003) CFTR channels, mean open burst duration (τ_b) of cut-ΔR(D1370N) proved largely ATP-independent: the time constant of macroscopic current relaxation following ATP removal (1342±72 ms; Fig. S2A, H), a measure of τ_b in zero ATP, was similar to steady-state τ_b of single channels in saturating (10 mM) ATP (1526±301 ms; Fig. 2A, B). Thus, ATP-dependence of P_o reflects ATP-dependence of its mean interburst duration (τ_{ib}). Importantly, in saturating (10 mM) ATP τ_{ib} is minimal, and bursting of this background construct is

reduced to a simple equilibrium ($C_1 \leftrightarrow O_1$; Fig. 1B, *red box*; see histograms of burst and interburst durations in Fig. S3) suitable for study by the REFER approach.

Timing of movements in composite site 2 of the NBD1-NBD2 interface

NBD2 Walker-A threonine 1246 makes important contributions to forming composite site 2 of the CFTR NBD1-NBD2 dimer, by contacting the γ-phosphate of ATP (PDBID: 3GD7). Moreover, this interfacial residue undergoes relative movement upon NBD dimerization, as reported by interaction of its sidechain across the dimer interface with that of opposing NBD1 residue R555 in open, but not closed, channels (Vergani et al., 2005). To test timing of relative movement at this NBD interface position, we created a series of mutants by replacing the native threonine with valine, proline, cysteine, asparagine, and alanine, respectively, and characterized their gating kinetics in inside-out single-channel patches superfused with 10 mM ATP (Fig. 2A). All of these perturbations dramatically reduced P_o (Fig. 2A and D) by prolonging mean interburst duration (τ_{ib}; Fig. 2A and C), i.e., by slowing channel opening rate ($k_{CO}=1/\tau_{ib}$). In comparison, mean open burst durations (τ_b), and hence closing rates ($1/\tau_b$), were less affected (Fig. 2A and B). Correspondingly, the Brønsted plot for position 1246 yielded a steep slope of $\Phi=0.97\pm0.19$ (Fig. 2D), indicating that this position moves very early during the pore opening conformational transition. Importantly, although mutations at position 1246 slightly reduce the affinity for ATP binding (Vergani et al., 2005), 10 mM ATP remained saturating for each of the mutants (Fig. S1C, *red bars*), confirming that their reduced opening rates indeed reflect slowing of step $C_1 \rightarrow O_1$ (k_{CO}, Fig. 1B).

Timing of movements at the NBD2-TMD interface

The four coupling helices at the NBD-TMD transmission interface undergo large movements between inward- and outward-facing conformations (Dawson and Locher, 2006; Hohl et al., 2012). Due to the domain swapping observed in ABC exporters, CH2 of TMD1 (residues 270-274) is in contact with NBD2 (He et al., 2008), and tyrosine 275 at the C-terminal end of CH2 is part of a conserved aromatic cluster important for NBD2-TMD interactions (Mornon et al., 2008). To test timing of motions at the NBD2-TMD transmission interface, we substituted phenylalanine, glutamate, lysine,

leucine, and serine, respectively, for tyrosine 275, and studied gating of single mutant channels in 10 mM ATP (Fig. 3A). Perturbations at position 275 caused modest changes in P_o, but in both directions (Fig. 3A, D). Kinetic analysis revealed a clear tendency for opposing effects on channel closing and opening rates, both contributing about equally to changes in P_o: lengthened τ_b was mostly associated with shortened τ_{ib}, and (in Y275L) shortened τ_b with lengthened τ_{ib} (Fig. 3B-C). Changes in opening rate ($1/\tau_{ib}$) again reflected changes in rate k_{CO} (Fig. 1B), since 10 mM ATP remained saturating for each mutant (Fig. S1C, *violet bars*). These coupled changes in opening and closing rates resulted in a Brønsted plot with an intermediate slope of Φ=0.50±0.13 (Fig. 3D), indicating that position 275 has not yet reached its final open-like position in the opening transition state.

Timing of movements in the pore region

Mutations of several pore residues were reported to affect gating (Zhang et al., 2000; Beck et al., 2008; Bai et al., 2010; Gao et al., 2013), indicating gating-related movements at these pore positions. To study the timing of such movements, we chose position 348 in transmembrane helix 6, because mutations here profoundly affected P_o without major effects on conductance (Bai et al., 2010), making it an attractive target for single-channel gating studies. To perturb position 348, we systematically replaced the native methionine with isoleucine, lysine, cysteine, asparagine, or alanine, and recorded single-channel currents of the mutants in 10 mM ATP (Fig. 4A), a saturating concentration for all constructs (Fig. S1C, *blue bars*). Except for the lysine substitution, perturbations at position 348 all dramatically reduced P_o (Fig. 4A, D), and this effect was in every case due to speeding of closing rate (reduction in τ_b, Fig. 1B), with little change in opening rate ($1/\tau_{ib}$, cf., Fig. 4C). Interestingly, the M348K mutation only marginally affected gating (Fig. 4A-D), but increased the affinity for pore block by ATP, as reported by pronounced flickery block of single-channel currents in 10 mM ATP (Fig. 4A), a bell-shaped ATP dose-dependence of macroscopic currents (cf., Fig. S1C, *second blue bar*), and a current overshoot upon ATP removal from macroscopic patches reflecting rapid unblock (Fig. S2F). Of note, even for M348K, the macroscopic current relaxation time constant following ATP removal (i.e., τ_b in zero ATP; Fig. S2G) remained comparable to steady-state τ_b: thus, even pronounced flickery block of M348K by 10 mM ATP does not delay pore closure, consistent with

earlier demonstration that the gate, located on the extracellular side, can readily close while large organic anion blockers remain bound in the intracellular vestibule (Csanády and Torocsik, 2014). We also replaced the methionine with glutamate, but this M348E mutant could not be studied at a single-channel level due to the presence of subconductance states; however, the rate of macroscopic current relaxation upon ATP removal attested to an acceleration of M348E closing rate comparable to that of the I, C, N, and A mutants (Fig. S2G, H). This speeding of non-hydrolytic closure (step $O_1 \rightarrow C_1$ in Fig. 1B, rate k_{OC}) by perturbations at position 348, with little effect on opening rate, led to a Brønsted plot with a small slope of Φ=0.20±0.12 (Fig. 4D), indicating that this pore region still resembles its closed-state conformation in the opening transition state.

Timing of movements in the narrow region of the pore studied by anion substitution

Previous accessibility studies outlined a short narrow region of the pore, confined to approximately one helical turn of pore-forming transmembrane helices 1 (residues 102-106), 6 (residues 337-341), 11 (residues 1115-1118), and 12 (residues 1130-36) (Beck et al., 2008; Fatehi and Linsdell, 2009; El Hiani and Linsdell, 2010; Bai et al., 2010; Qian et al., 2011; Wang et al., 2011; Gao et al., 2013; Wang et al., 2014b). This narrow region was shown to act as a lyotropic "selectivity filter" which provides sites of interaction (T338, S341, S1118, T1134) for permeating anions (McDonough et al., 1994; Linsdell et al., 2000; Linsdell, 2001; Zhang et al., 2000; McCarty and Zhang, 2001). Intriguingly, replacement of chloride with nitrate affects CFTR gating (Yeh et al., 2015), suggesting that interactions of permeating anions with residues lining the "filter" region of the open pore energetically contribute to open-state stability. Thus, replacement of chloride with other permeant anions might be viewed as a structural perturbation of the "selectivity filter". We therefore studied changes in the pattern of single-channel gating of our background construct cut-ΔR(D1370N) in response to sudden replacement of cytosolic chloride with nitrate, bromide, or formate. Of note, in these experiments gating in chloride and in the replacement anion could be compared within the same patch (Fig. 5A): this arrangement eliminates any uncertainties about perturbation-induced fractional changes in opening rate, precise estimation of which is normally dependent on correct judgement of the number of active channels in each patch.

In addition to documented reductions in unitary conductance (Linsdell, 2001), perturbations of the filter by replacement of permeating chloride with nitrate, bromide, or formate all affected gating: nitrate and bromide which bind more tightly in the pore (Linsdell, 2001) increased P_o, while formate which binds less tightly (Linsdell, 2001) decreased it (Fig. 5A, D). Importantly, both gating effects primarily reflected changes in τ_b (Fig. 5B), i.e., in rate k_{OC} of step $O_1 \rightarrow C_1$ (Fig. 1B), with smaller changes in τ_{ib} (Fig. 5C); the observations on nitrate replicated those of (Yeh et al., 2015). The slope of the Brønsted plot constructed from these data yielded Φ=0.28±0.03 (Fig. 5D), similar to that of position 348. These ionic replacement studies therefore provide independent support for a small Φ value in the pore, confirming late movement of this region during opening.

Discussion

The general structural orientations of protein domains in the stable closed and open states of the CFTR channel have been delineated by a large body of previous work. Thus, the preponderance of evidence has established that the channel's closed state corresponds to a dissociated NBD dimer interface (Vergani et al., 2005; Mense et al., 2006; Chaves and Gadsby, 2015) and inward-facing TMDs (Bai et al., 2011; Cui et al., 2014; Wang et al., 2014a), with the closed gate located on the extracellular side of the membrane (Bai et al., 2011; Cui et al., 2014; Csanády and Torocsik, 2014; Gao and Hwang, 2015). Similarly, evidence suggests that in the open state the NBDs are dimerized (Vergani et al., 2005; Mense et al., 2006; Chaves and Gadsby, 2015), while a conducting pore is formed by outward-facing TMDs (Bai et al., 2011; Cui et al., 2014; Wang et al., 2014a). Consequently, several homology models of closed- and open-state CFTR have been constructed based on crystal structures of homologous ABC exporters in their inward- and outward-facing conformations (e.g.; (Mornon et al., 2009; Corradi et al., 2015); Fig. 6B, *left* and *right*). In contrast, far less is known about the nature and relative timing of the sub-microsecond molecular motions that drive the channel from its closed- to its open-state conformation.

Here we have adapted the REFER technique to obtain new insight into the dynamics of ATP-dependent gating conformational changes of the CFTR protein: careful choice of the background construct (see below) allowed selective examination of the channel opening process (step $C_1 \rightarrow O_1$, Fig. 1B). The strikingly different Φ values obtained for our three target positions define a clear spatial gradient along the protein's longitudinal axis from cytoplasm to cell exterior: the very high Φ value of ~0.97 for site-2 NBD interface position 1246 (Fig. 2E, Fig. 6A, *red*) stands in stark contrast to the low Φ value of ~0.20 for intra-pore position 348. For the pore region a similarly small Φ value emerges also from our anion substitution studies: replacement of permeating chloride with anions such as nitrate and bromide, which bind more tightly to the pore (as indicated by permeability ratio measurement; Linsdell, 2001), clearly stabilize the open state, whereas formate, which binds less tightly than chloride (Linsdell, 2001), destabilizes it (Fig. 5B). Although the precise location at which permeating anions act to affect CFTR gating is unknown, this strong positive correlation between anion binding affinity in the

filter and open-state stability does support the notion that the gating effects are caused by interactions of the anions with residues located somewhere in the pore. It is notable that the effects of ionic replacement on open-closed equilibrium were in each case associated with changes in closing, rather than opening rates (Fig. 5A-C), implying that the stability of the transition state, relative to the closed state, is less sensitive to the permeating anion species. Insofar as pore-anion interactions are expected to change between the closed and open state, the implication is that in the transition state these interactions resemble those in the closed state: i.e., the pore is closed. The Brønsted plots for ionic replacement and for the 348 position closely agree with each other, and the combined data are well fitted by a single line with a slope of 0.23±0.05 (Fig. 6A, *blue*). Compared to the Φ values for the NBD1-NBD2 interface and the pore, which are close to the smallest and highest possible values for this parameter, respectively, the slope of ~0.50 of the Brønsted plot for NBD-TMD interface position 275 (Fig. 6A, *violet*) appears intermediate, distinctly different from the two extremes. This spatially organized Φ value gradient provides support for the interpretation that for conformational changes of folded proteins the relative magnitude of Φ reflects relative timing of ordered sequential movements (Zhou et al., 2005; Auerbach, 2007), albeit on the sub-microsecond time scale, as opposed to probabilities of taking alternative kinetic pathways known to exist for more random processes such as protein folding (cf., (Purohit et al., 2013)). For the CFTR pore opening transition this spatial Φ-gradient implies a conformational wave (Fig. 6B, *large vertical arrow*) initiated by tightening of the NBD dimer around site 2, and propagated with some delay through the NBD-TMD interface to eventually result in pore opening.

Furthermore, this set of Φ values provides strong global constraints for the structure of the actual transition state, the highest free-energy intermediate of the channel opening process (Fig. 6B, *center*). For the NBD interface the Φ value of ~1 indicates that it has already reached its open-state conformation, i.e., the tight dimer is already formed (cf., (Vergani et al., 2005)). In contrast, the low Φ value of ~0.2 for the pore region implies it is still in its closed-like, inward-facing conformation. Finally, the intermediate Φ value of ~0.5 for position 275 suggests that in the transition state coupling helix 2 is just on the move: it has already left its closed-like, but has not yet reached its open-like conformation (Fig. 6B, *center*, *bent rods*). This transition state architecture, which emerges from direct

measurements of relative timing of movements, confirms a previous speculation based on interpretation of enthalpy and entropy changes determined for the opening transition state (Csanády et al., 2006), but refutes the alternative proposition that during opening all structural reorganizations in the cytoplasmic loops are completed in the channel closed state (Aleksandrov et al., 2009). The large molecular strain which must arise at the NBD-TMD interface is the most likely cause of the very high enthalpy of the opening transition state ($\Delta H^{\ddagger}$ =117 kJ/mol), and is only partially compensated by an entropy increase ($T\Delta S^{\ddagger} \geq 41$ kJ/mol) suggested to reflect dehydration of the closing NBD dimer interface (i.e., dispersal of the layer of ordered water molecules into the disordered bulk solution) (Csanády et al., 2006). Evidently, transition-state free energy ($\Delta G^{\ddagger} = \Delta H^{\ddagger} - T\Delta S^{\ddagger}$) of wild-type CFTR is still very high, as witnessed by its very slow opening rate of ~1 s^{-1}, >4 orders of magnitude slower than for the ligand-gated nicotinic acetylcholine receptor (e.g., (Jackson et al., 1983)). Moreover, it is this transient conformation of CFTR which is further destabilized (relative to the closed state) by NBD-TMD interface mutation ΔF508, causing the severe gating defect of this most common CF-associated mutant. Indeed, stabilization of the opening transition state seems an attractive strategy for designing potentiator compounds that stimulate gating of ΔF508 CFTR: thus, 5-Nitro-2-(3-phenylpropylamino)benzoate, one of its most efficacious potentiators (albeit with a pore blocking side effect; Wang et al., 2005), increases ΔF508 CFTR opening rate by precisely that mechanism (Csanády and Torocsik, 2014).

Successful adaptation of the classical REFER approach to studying CFTR gating dynamics rested on three important innovations.

First, rather than focusing on the kinetics of pore opening and closure (cf., (Scott-Ward et al., 2007)), the durations of *bursts* of openings and of long *interburst* closures were analyzed here, as the latter reflect conformational states of the pore associated with specific conformations of the NBDs: bursts are linked to tightly dimerized NBDs, while interburst closures reflect dissociation of the NBD interface around site 2 (Vergani et al., 2005; Chaves and Gadsby, 2015). The duration of the "active" pore conformation induced by a single ATP occlusion event at site 2 is also reflected by the time constant of macroscopic current relaxation upon sudden removal of ATP. Indeed, for all of our constructs which afforded macroscopic recordings, such macroscopic current relaxation time constants

(Fig. S2) were in good agreement with the mean burst durations obtained by conventional burst analysis of steady-state single-channel recordings (Figs. 2B-5B), confirming that τ_b indeed reflects the duration of an activated state of the pore induced by a single ATP occlusion event.

Second, CFTR bursting follows a non-equilibrium cycle ((Gunderson and Kopito, 1995; Csanády et al., 2010); cf., Fig. 1B) to which REFER analysis is not applicable (Csanády, 2009). To study the pore opening step, we therefore employed the D1370N background mutation which truncates the gating cycle to an equilibrium scheme (Fig. 1B, *red frame*). Indeed, this is the key feature which distinguishes our approach from previous studies, and is responsible for its very different outcome. This is because in the normal hydrolytic background, mutation-induced changes in the rate of slow non-hydrolytic closure (rate k_{OC}, Fig. 1B) remain unnoticed as long as the much faster hydrolytic pathway (rate $O_1 \rightarrow O_2$, Fig. 1B) dominates pore closure. It is therefore not surprising that structural perturbations introduced into the nucleotide binding sites and several TMD/NBD interface positions of WT CFTR affected only channel opening rates, yielding apparent Φ values of ~1 for all positions tested (Aleksandrov et al., 2009). Similarly, previous studies identified several pore mutations that affected gating (e.g., (Beck et al., 2008; Bai et al., 2010)), but in the framework of a hydrolytic gating cycle even the large, almost an order of magnitude, acceleration of non-hydrolytic closing rates reported here for mutations at position 348 so far evaded detection. Of note, the ΔF508 mutation also greatly accelerates non-hydrolytic closure (Jih et al., 2011) – suggesting an intermediate Φ value for position 508 –, yet under normal hydrolytic conditions ΔF508 closing rate is unaffected (Miki et al., 2010; Kopeikin et al., 2014).

Third, removal of the R domain eliminated potential confounding effects of altered R-domain mediated gating regulation in our target-site mutants: not only does the non-phosphorylated R domain *inhibit* channel gating, but the phosphorylated R domain also mediates substantial *stimulation* of channel P_o (Winter and Welsh, 1997; Csanády et al., 2000), through mechanisms which are poorly understood. In that regard our cut-ΔR background construct, pared down to the canonical ABC domains, reduces complexity: in addition to obviating the need for prior phosphorylation by PKA, gating of cut-ΔR CFTR is regulated only by ATP, similarly to the transport cycle of ABC exporters. Thus, our Φ-value map likely bears relevance to the transition state for the inward- to outward-facing

transition in this broader family of CFTR relatives. Because gating of cut-ΔR(D1370N), like that of WT CFTR, is strictly ATP dependent (Figs. S1-S2), our conclusions do not necessarily apply to the mechanism of the extremely infrequent spontaneous openings observable in the absence of ATP that are promoted by certain mutations (Wang et al., 2010) and drugs (Jih and Hwang, 2013).

In conclusion, we have provided an initial characterization of the CFTR opening transition-state structure which could serve as a drug target for treating CF, and developed a technique to directly measure timing of movements in distinct regions of the CFTR protein during the sub-microsecond process of channel opening. By further refining the Φ value map, this approach might be used in the future to define regions which move as a rigid body (cf., (Purohit et al., 2013; Purohit et al., 2015)), or to shed light on potentially asynchronous movements at the level of the ATP binding sites, the coupling helices, or the TM helices that form the pore.

Experimental Procedures

pGEMHE-CFTR(837-1480(D1370N)) was constructed from pGEMHE-CFTR(837-1480), mutations at positions 275 and 348 were introduced into pGEMHE-CFTR(1-633) (Csanády et al., 2000), and mutations at position 1246 into pGEMHE-CFTR(837-1480(D1370N)) using Stratagene QuickChange. cDNA was transcribed *in vitro* using T7 polymerase, and 0.1-10 ng cRNA for both CFTR segments were co-injected into *Xenopus laevis* oocytes. Currents were recorded at 25^{o}C in inside-out patches excised from oocytes 1-5 days after RNA injection. Pipette solution contained (in mM) 136 NMDG-Cl, 2 $MgCl_2$, 5 HEPES, pH=7.4 with NMDG. The continuously flowing bath solution could be exchanged with a time constant <100 ms. Standard (chloride-based) bath solution contained 134 NMDG-Cl, 2 $MgCl_2$, 5 HEPES, 0.5 EGTA, pH=7.1 with NMDG. For anion substitution experiments NMDG-Cl and $MgCl_2$ were replaced by NMDG and $Mg(OH)_2$, and the solution titrated to pH=7.1 with nitric, hydrobromic, or formic acid, respectively. MgATP (Sigma) was added from a 400-mM aqueous stock solution (pH=7.1 with NMDG). Unitary CFTR currents in 10 mM MgATP were recorded at -80 mV (-100 mV for formate currents) (EPC7, Heka Elektronik) at a bandwidth of 2 kHz, and digitized at 10 kHz. Single-channel patches were identified as very long (typically 15 min - 1 h) recordings without superimposed channel openings. For T1246 mutants strong stimulation by 2'-deoxy-ATP at the end of each experiment was used to facilitate correct estimation of the number of active channels in the patch (Fig. S4). To reconstruct bursts and interbursts, currents from patches containing no superimposed channel openings were refiltered at 20 Hz (10 Hz for anion substitution experiments), idealized by half-amplitude threshold crossing, and brief closures suppressed (Fig. S3) using the method of (Magleby and Pallotta, 1983). Opening (k_{CO}) and closing (k_{OC}) rates were defined as $1/\tau_{ib}$ and $1/\tau_b$, respectively, and K_{eq} as k_{CO}/k_{OC}. All data are given as mean±SEM of measurements from ≥4 (typically 5-8) long segments of single-channel recordings, from 4-13 patches for each mutant; in the face of alternating periods of lower and higher activity typical to CFTR (Bompadre et al., 2005), several hours of total recording for each construct were obtained to ensure unbiased sampling of average gating behaviour. Macroscopic current ratios between 3 and 10 mM ATP were used to verify saturation by 10 mM ATP (Fig. S1). Time constants of macroscopic current relaxations upon ATP removal were obtained from single-exponential fits (Fig. S2).

Author Contributions

Conceptualization, Methodology, Software, L.C., Resources, Investigation, Formal Analysis, B.S. and D.C., Supervision, Writing, L.C.

Acknowledgements

We thank Beáta Törőcsik for generous help and guidance in molecular biology, and David Gadsby and Paola Vergani for critical review and discussions. Supported by MTA Lendület grant LP2012-39/2012, a Research Grant from the Cystic Fibrosis Foundation, and an International Early Career Scientist grant from the Howard Hughes Medical Institute to L.C.

References

Aleksandrov, A.A., Cui, L., and Riordan, J.R. (2009). Relationship between nucleotide binding and ion channel gating in cystic fibrosis transmembrane conductance regulator. J. Physiol *587*, 2875-2886.

Aleksandrov, L., Aleksandrov, A.A., Chang, X.B., and Riordan, J.R. (2002). The First Nucleotide Binding Domain of Cystic Fibrosis Transmembrane Conductance Regulator Is a Site of Stable Nucleotide Interaction, whereas the Second Is a Site of Rapid Turnover. J. Biol. Chem *277*, 15419-15425.

Auerbach, A. (2007). How to turn the reaction coordinate into time. J. Gen. Physiol *130*, 543-546.

Bai, Y.H., Li, M., and Hwang, T.C. (2010). Dual roles of the sixth transmembrane segment of the CFTR chloride channel in gating and permeation. J. Gen. Physiol *136*, 293-309.

Bai, Y.H., Li, M., and Hwang, T.C. (2011). Structural basis for the channel function of a degraded ABC transporter, CFTR (ABCC7). J. Gen. Physiol *138*, 495-507.

Basso, C., Vergani, P., Nairn, A.C., and Gadsby, D.C. (2003). Prolonged nonhydrolytic interaction of nucleotide with CFTR's NH2-terminal nucleotide binding domain and its role in channel gating. J. Gen. Physiol *122*, 333-348.

Beck, E.J., Yang, Y., Yaemsiri, S., and Raghuram, V. (2008). Conformational changes in a pore-lining helix coupled to cystic fibrosis transmembrane conductance regulator channel gating. J. Biol. Chem *283*, 4957-4966.

Bompadre, S.G., Ai, T., Cho, J.H., Wang, X., Sohma, Y., Li, M., and Hwang, T.C. (2005). CFTR gating I: Characterization of the ATP-dependent gating of a phosphorylation-independent CFTR channel (DeltaR-CFTR). J. Gen. Physiol *125*, 361-375.

Bozoky, Z., Krzeminski, M., Muhandiram, R., Birtley, J.R., Al Zahrani, A., Thomas, P.J., Frizzell, R.A., Ford, R.C., and Forman-Kay, J.D. (2013). Regulatory R region of the CFTR chloride channel is a dynamic integrator of phospho-dependent intra- and intermolecular interactions. Proc. Natl. Acad. Sci. USA *110*, E4427-E4436.

Chaves, L.A.P. and Gadsby, D.C. (2015). Cysteine accessibility probes timing and extent of NBD separation along the dimer interface in gating CFTR channels. J. Gen. Physiol *145*, 261-283.

Cheng, S.H., Gregory, R.J., Marshall, J., Paul, S., Souza, D.W., White, G.A., Oriordan, C.R., and Smith, A.E. (1990). Defective Intracellular-Transport and Processing of Cftr Is the Molecular-Basis of Most Cystic-Fibrosis. Cell *63*, 827-834.

Corradi, V., Vergani, P., and Tieleman, D.P. (2015). Cystic fibrosis transmembrane conductance regulator (CFTR): closed and open state channel models. J. Biol. Chem. pii: jbc.M115.665125. PMID:26229102

Csanády, L. (2009). Application of rate-equilibrium free energy relationship analysis to nonequilibrium ion channel gating mechanisms. J. Gen. Physiol *134*, 129-136.

Csanády, L., Chan, K.W., Seto-Young, D., Kopsco, D.C., Nairn, A.C., and Gadsby, D.C. (2000). Severed channels probe regulation of gating of cystic fibrosis transmembrane conductance regulator by its cytoplasmic domains. J. Gen. Physiol *116*, 477-500.

Csanády, L., Nairn, A.C., and Gadsby, D.C. (2006). Thermodynamics of CFTR channel gating: a spreading conformational change initiates an irreversible gating cycle. J. Gen. Physiol *128*, 523-533.

Csanády, L. and Torocsik, B. (2014). Catalyst-like modulation of transition states for CFTR channel opening and closing: New stimulation strategy exploits nonequilibrium gating. J. Gen. Physiol *143*, 269-287.

Csanády, L., Vergani, P., and Gadsby, D.C. (2010). Strict coupling between CFTR's catalytic cycle and gating of its Cl- ion pore revealed by distributions of open channel burst durations. Proc. Natl. Acad. Sci. USA *107*, 1241-1246.

Cui, G.Y., Rahman, K.S., Infield, D.T., Kuang, C., Prince, C.Z., and McCarty, N.A. (2014). Three charged amino acids in extracellular loop 1 are involved in maintaining the outer pore architecture of CFTR. J. Gen. Physiol *144*, 159-179.

Dawson, R.J.P. and Locher, K.P. (2006). Structure of a bacterial multidrug ABC transporter. Nature *443*, 180-185.

El Hiani, Y. and Linsdell, P. (2010). Changes in Accessibility of Cytoplasmic Substances to the Pore Associated with Activation of the Cystic Fibrosis Transmembrane Conductance Regulator Chloride Channel. J. Biol. Chem *285*, 32126-32140.

Fatehi, M. and Linsdell, P. (2009). Novel Residues Lining the CFTR Chloride Channel Pore Identified by Functional Modification of Introduced Cysteines. J. Membr. Biol *228*, 151-164.

Gao, X., Bai, Y., and Hwang, T.C. (2013). Cysteine Scanning of CFTR's First Transmembrane Segment Reveals Its Plausible Roles in Gating and Permeation. Biophys. J *104*, 786-797.

Gao, X.L. and Hwang, T.C. (2015). Localizing a gate in CFTR. Proc. Natl. Acad. Sci. USA *112*, 2461-2466.

Gunderson, K.L. and Kopito, R.R. (1995). Conformational states of CFTR associated with channel gating: the role ATP binding and hydrolysis. Cell *82*, 231-239.

He, L.H., Aleksandrov, A.A., Serohijos, A.W.R., Hegedus, T., Aleksandrov, L.A., Cui, L., Dokholyan, N.V., and Riordan, J.R. (2008). Multiple membrane-cytoplasmic domain contacts in the cystic fibrosis transmembrane conductance regulator (CFTR) mediate regulation of channel gating. J. Biol. Chem *283*, 26383-26390.

Hohl, M., Briand, C., Grutter, M.G., and Seeger, M.A. (2012). Crystal structure of a heterodimeric ABC transporter in its inward-facing conformation. Nat. Struct. Mol. Biol *19*, 395-402.

Hopfner, K.P., Karcher, A., Shin, D.S., Craig, L., Arthur, L.M., Carney, J.P., and Tainer, J.A. (2000). Structural biology of Rad50 ATPase: ATP-driven conformational control in DNA double-strand break repair and the ABC-ATPase superfamily. Cell *101*, 789-800.

Hrycyna, C.A., Ramachandra, M., Germann, U.A., Cheng, P.W., Pastan, I., and Gottesman, M.M. (1999). Both ATP sites of human P-glycoprotein are essential but not symmetric. Biochemistry *38*, 13887-13899.

Hung, L.W., Wang, I.X., Nikaido, K., Liu, P.Q., Ames, G.F., and Kim, S.H. (1998). Crystal structure of the ATP-binding subunit of an ABC transporter. Nature *396*, 703-707.

Jackson, M.B., Wong, B.S., Morris, C.E., Lecar, H., and Christian, C.N. (1983). Successive openings of the same acetylcholine receptor channel are correlated in open time. Biophys. J *42*, 109-114.

Jih, K.Y. and Hwang, T.C. (2013). Vx-770 potentiates CFTR function by promoting decoupling between the gating cycle and ATP hydrolysis cycle. Proc. Natl. Acad. Sci. USA *110*, 4404-4409.

Jih, K.Y., Li, M., Hwang, T.C., and Bompadre, S.G. (2011). The most common cystic fibrosis-associated mutation destabilizes the dimeric state of the nucleotide-binding domains of CFTR. J. Physiol *589*, 2719-2731.

Kopeikin, Z., Yuksek, Z., Yang, H.Y., and Bompadre, S.G. (2014). Combined effects of VX-770 and VX-809 on several functional abnormalities of F508del-CFTR channels. J. Cyst. Fibros. *13, 508-514.*

Linsdell, P. (2001). Relationship between anion binding and anion permeability revealed by mutagenesis within the cystic fibrosis transmembrane conductance regulator chloride channel pore. J. Physiol *531*, 51-66.

Linsdell, P., Evagelidis, A., and Hanrahan, J.W. (2000). Molecular determinants of anion selectivity in the cystic fibrosis transmembrane conductance regulator chloride channel pore. Biophys. J *78*, 2973-2982.

Locher, K.P. (2009). Structure and mechanism of ATP-binding cassette transporters. Philos. T. R. Soc. B *364*, 239-245.

Magleby, K.L. and Pallotta, B.S. (1983). Burst kinetics of single calcium-activated potassium channels in cultured rat muscle. J. Physiol *344*, 605-623.

McCarty, N.A. and Zhang, Z.R. (2001). Identification of a region of strong discrimination in the pore of CFTR. Am. J. Physiol.-Lung C *281*, L852-L867.

McDonough, S., Davidson, N., Lester, H.A., and McCarty, N.A. (1994). Novel Pore-Lining Residues in Cftr That Govern Permeation and Open-Channel Block. Neuron *13*, 623-634.

Mense, M., Vergani, P., White, D.M., Altberg, G., Nairn, A.C., and Gadsby, D.C. (2006). In vivo phosphorylation of CFTR promotes formation of a nucleotide-binding domain heterodimer. EMBO J *25*, 4728-4739.

Miki, H., Zhou, Z., Li, M., Hwang, T.C., and Bompadre, S.G. (2010). Potentiation of Disease-associated Cystic Fibrosis Transmembrane Conductance Regulator Mutants by Hydrolyzable ATP Analogs. J. Biol. Chem *285*, 19967-19975.

Mitra, A., Cymes, G.D., and Auerbach, A. (2005). Dynamics of the acetylcholine receptor pore at the gating transition state. Proc. Natl. Acad. Sci. USA *102*, 15069-15074.

Moody, J.E., Millen, L., Binns, D., Hunt, J.F., and Thomas, P.J. (2002). Cooperative, ATP-dependent association of the nucleotide binding cassettes during the catalytic cycle of ATP-binding cassette transporters. J. Biol. Chem *277*, 21111-21114.

Mornon, J.P., Lehn, P., and Callebaut, I. (2008). Atomic model of human cystic fibrosis transmembrane conductance regulator: Membrane-spanning domains and coupling interfaces. Cell. Mol. Life Sci *65*, 2594-2612.

Mornon, J.P., Lehn, P., and Callebaut, I. (2009). Molecular models of the open and closed states of the whole human CFTR protein. Cell. Mol. Life Sci *66*, 3469-3486.

O'Sullivan, B.P. and Freedman, S.D. (2009). Cystic fibrosis. Lancet *373*, 1891-1904.

Purohit, P., Chakraborty, S., and Auerbach, A. (2015). Function of the M1 pi-helix in endplate receptor activation and desensitization. J. Physiol *593*, 2851-2866.

Purohit, P., Gupta, S., Jadey, S., and Auerbach, A. (2013). Functional anatomy of an allosteric protein. Nat. Commun *4*, 2984.

Purohit, P., Mitra, A., and Auerbach, A. (2007). A stepwise mechanism for acetylcholine receptor channel gating. Nature *446*, 930-933.

Qian, F., El Hiani, Y., and Linsdell, P. (2011). Functional arrangement of the 12th transmembrane region in the CFTR chloride channel pore based on functional investigation of a cysteine-less CFTR variant. Pflugers Arch *462*, 559-571.

Rai, V., Gaur, M., Shukla, S., Shukla, S., Ambudkar, S.V., Komath, S.S., and Prasad, R. (2006). Conserved Asp327 of walker B motif in the N-terminal nucleotide binding domain (NBD-1) of Cdr1p of Candida albicans has acquired a new role in ATP hydrolysis. Biochemistry *45*, 14726-14739.

Riordan, J.R., Rommens, J.M., Kerem, B., Alon, N., Rozmahel, R., Grzelczak, Z., Zielenski, J., Lok, S., Plavsic, N., Chou, J.L., et al. (1989). Identification of the cystic fibrosis gene: cloning and characterization of complementary DNA. Science *245*, 1066-1073.

Scott-Ward, T.S., Cai, Z., Dawson, E.S., Doherty, A., Da Paula, A.C., Davidson, H., Porteous, D.J., Wainwright, B.J., Amaral, M.D., Sheppard, D.N., and Boyd, A.C. (2007). Chimeric constructs endow the human CFTR Cl- channel with the gating behavior of murine CFTR. Proc. Natl. Acad. Sci. USA *104*, 16365-16370.

Smith, P.C., Karpowich, N., Millen, L., Moody, J.E., Rosen, J., Thomas, P.J., and Hunt, J.F. (2002). ATP binding to the motor domain from an ABC transporter drives formation of a nucleotide sandwich dimer. Mol. Cell *10*, 139-149.

Tabcharani, J.A., Chang, X.B., Riordan, J.R., and Hanrahan, J.W. (1991). Phosphorylation-regulated Cl- channel in CHO cells stably expressing the cystic fibrosis gene. Nature *352*, 628-631.

Urbatsch, I.L., Beaudet, L., Carrier, I., and Gros, P. (1998). Mutations in either nucleotide-binding site of P-glycoprotein (Mdr3) prevent vanadate trapping of nucleotide at both sites. Biochemistry *37*, 4592-4602.

Vergani, P., Lockless, S.W., Nairn, A.C., and Gadsby, D.C. (2005). CFTR channel opening by ATP-driven tight dimerization of its nucleotide-binding domains. Nature *433*, 876-880.

Vergani, P., Nairn, A.C., and Gadsby, D.C. (2003). On the mechanism of MgATP-dependent gating of CFTR Cl- channels. J. Gen. Physiol *121*, 17-36.

Wang, W., He, Z., O'Shaughnessy, T.J., Rux, J., and Reenstra, W.W. (2002). Domain-domain associations in cystic fibrosis transmembrane conductance regulator. Am. J. Physiol. Cell Physiol *282*, C1170-C1180.

Wang, W., Li, G., Clancy, J.P., and Kirk, K.L. (2005). Activating cystic fibrosis transmembrane conductance regulator channels with pore blocker analogs. J. Biol. Chem *280*, 23622-23630.

Wang, W., Roessler, B.C., and Kirk, K.L. (2014a). An Electrostatic Interaction at the Tetrahelix Bundle Promotes Phosphorylation-dependent Cystic Fibrosis Transmembrane Conductance Regulator (CFTR) Channel Opening. J. Biol. Chem *289*, 30364-30378.

Wang, W., Wu, J.P., Bernard, K., Li, G., Wang, G.Y., Bevensee, M.O., and Kirk, K.L. (2010). ATP-independent CFTR channel gating and allosteric modulation by phosphorylation. Proc. Natl. Acad. Sci. USA *107*, 3888-3893.

Wang, W.Y., El Hiani, Y., and Linsdell, P. (2011). Alignment of transmembrane regions in the cystic fibrosis transmembrane conductance regulator chloride channel pore. J. Gen. Physiol *138*, 165-178.

Wang, W.Y., El Hiani, Y., Rubaiy, H.N., and Linsdell, P. (2014b). Relative contribution of different transmembrane segments to the CFTR chloride channel pore. Pflugers Arch *466*, 477-490.

Winter, M.C., Sheppard, D.N., Carson, M.R., and Welsh, M.J. (1994). Effect of ATP concentration on CFTR Cl- channels: a kinetic analysis of channel regulation. Biophys. J *66*, 1398-1403.

Winter, M.C. and Welsh, M.J. (1997). Stimulation of CFTR activity by its phosphorylated R domain. Nature *389*, 294-296.

Yeh, H.I., Yeh, J.T., and Hwang, T.C. (2015). Modulation of CFTR gating by permeant ions. J. Gen. Physiol *145*, 47-60.

Zeltwanger, S., Wang, F., Wang, G.T., Gillis, K.D., and Hwang, T.C. (1999). Gating of cystic fibrosis transmembrane conductance regulator chloride channels by adenosine triphosphate hydrolysis. Quantitative analysis of a cyclic gating scheme. J. Gen. Physiol *113*, 541-554.

Zhang, Z.R., McDonough, S.I., and McCarty, N.A. (2000). Interaction between permeation and gating in a putative pore domain mutant in the cystic fibrosis transmembrane conductance regulator. Biophys. J *79*, 298-313.

Zhou, Y., Pearson, J.E., and Auerbach, A. (2005). Phi-value analysis of a linear, sequential reaction mechanism: theory and application to ion channel gating. Biophys. J *89*, 3680-3685.

Figure Legends

Figure 1. Choice of a suitable background construct for REFER analysis. *A*, Domain organizations of WT (*top*) and cut-ΔR(D1370N) (*bottom*) CFTR: TMDs (*gray*), intracellular loops containing coupling helices (*light violet*), NBD1 (*green*), NBD2 (*blue*), R domain (*magenta*), membrane (*yellow*). *Colored circles* identify target positions. The D1370N mutation in NBD2 is depicted by a *red star*. *B*, Cartoon representation of the CFTR gating cycle. ATP-bound closed channels (C_1) open to a prehydrolytic open state (O_1). During most openings ATP is hydrolyzed at composite site 2 (state O_2), prompting NBD dimer dissociation and pore closure (to state C_2) followed by ADP-ATP exchange (to state C_1). Color coding as in *A*, ATP (*yellow circles*), ADP (*orange crescents*). The D1370N mutation abrogates ATP hydrolysis (*red cross*), and confines gating in saturating ATP to a simple $C_1 \leftrightarrow O_1$ equilibrium (*red box*). Target positions color coded as in *A*.

Figure 2. Timing of motion at position 1246 of the NBD1-NBD2 interface. *A*, Inward single-channel currents of the cut-ΔR(D1370N) CFTR background construct (*top trace*), and of channels bearing mutations T1246V, T1246P, T1246C, T1246N, and T1246A, respectively, in the same background. Currents were recorded at -80 mV, in symmetrical 140 mM Cl^-; *dashes* on the left mark zero-current level. *B-D*, Mean burst (*B*, τ_b) and interburst (*C*, τ_{ib}) durations and open probabilities (*D*, P_o) of the six constructs in *A*. *Red horizontal lines* highlight the respective control values of the background construct. All data are shown as mean ± SEM (n = 4-28). *E*, Brønsted plot for position 1246. *Gray symbol* identifies the background construct (also in Figs. 3-5E). *Solid line* is a linear regression fit with slope Φ indicated.

Figure 3. Timing of motion at position 275 of the NBD2-TMD interface. *A*, Inward single-channel currents of the cut-ΔR(D1370N) CFTR background construct (*top trace*), and of channels bearing mutations Y275F, Y275E, Y275K, Y275L, and Y275S, respectively, in the same background. Currents were recorded at -80 mV, in symmetrical 140 mM Cl^-; *dashes* on the left mark zero-current level. *B-D*, Mean burst (*B*, τ_b) and interburst (*C*, τ_{ib}) durations and open probabilities (*D*, P_o) of the six constructs in *A*. *Red horizontal lines* highlight the respective control values of the background construct. All data

are shown as mean ± SEM (n = 9-28). *E*, Brønsted plot for position 275. *Solid line* is a linear regression fit with slope Φ indicated.

Figure 4. Timing of motion at position 348 in the pore region. *A*, Inward single-channel currents of the cut-ΔR(D1370N) CFTR background construct (*top trace*), and of channels bearing mutations M348I, M348K, M348C, M348N, and M348A, respectively, in the same background. Currents were recorded at -80 mV, in symmetrical 140 mM Cl^-; *dashes* on the left mark zero-current level. *B*-*D*, Mean burst (*B*, τ_b) and interburst (*C*, τ_{ib}) durations and open probabilities (*D*, P_o) of the six constructs in *A*. *Red horizontal lines* highlight the respective control values of the background construct. All data are shown as mean ± SEM (n = 4-28). *E*, Brønsted plot for position 348. *Solid line* is a linear regression fit with slope Φ indicated.

Figure 5. Timing of motion in the narrow region of the pore studied by anion replacement. *A*, Pairs of segments of inward single-channel current from three patches containing single cut-ΔR(D1370N) CFTR channels. Each patch was alternately exposed to bath solutions containing 140 mM of either chloride (*upper segments*) or a test anion (*lower segments*), as indicated to the right: chloride (Cl^-), bromide (Br^-), nitrate (Nt^-), formate (Fm^-). Currents in Cl^-, Br^-, and Nt^- were recorded at -80 mV, those in Fm^- at -100 mV; *dashes* on the left mark zero-current level. *B*-*D*, Mean burst (*B*, τ_b) and interburst (*C*, τ_{ib}) durations and open probabilities (*D*, P_o) in the presence of various test anions, each normalized to the value observed in chloride in the same patch. *Red horizontal lines* highlight the respective control values in chloride. All data are shown as mean ± SEM (n = 5-9). *E*, Brønsted plot for the narrow region of the pore, constructed from normalized opening rates and equilibrium constants in the presence of the four permeating anions tested. *Solid line* is a linear regression fit with slope Φ indicated.

Figure 6. Opening conformational wave and transition-state structure reported by Φ-value analysis. *A*, Merged normalized Brønsted plot for the pore region (*blue*). Fitting the ensemble of the normalized data for position 348 (*standing triangles*) and for the anion substitution experiments (*inverted triangles*) by linear regression (*solid blue line*) yielded the indicated slope value (Φ).

Brønsted plots for positions 1246 (*red*) and 275 (*violet*) are normalized versions of the plots in Figs. 2E and 3E, respectively. The point representing the cut-ΔR(D1370N) background construct in chloride is highlighted by a black circle. *B*, Ribbon representation of CFTR homology models (Corradi et al., 2015) in the closed (*left*) and open (*right*) states based on (*left*) the inward-facing structure of TM287-288 (Hohl et al., 2012) and (*right*) the outward-facing structure of Sav1866 (Dawson and Locher, 2006), and cartoon depicting rough domain organization in the opening transition state (*center*). The three target positions are highlighted in spacefill on the models, and as *colored circles* in the cartoon. CFTR domain color coding follows that of Fig. 1; threonine 1246 (*red*), tyrosine 275 (*violet*), methionine 348 (*blue*). *Blue ribbons* in the homology models highlight segments 102-106 (TM1), 337-341 (TM6), 1115-1118 (TM11), and 1130-1134 (TM12), that form the narrow region of the pore (*blue ovals* in cartoon). Vertical colored arrow illustrates the direction and timing of the conformational wave during pore opening (early – *red*, late – *blue*).

Fig. 1

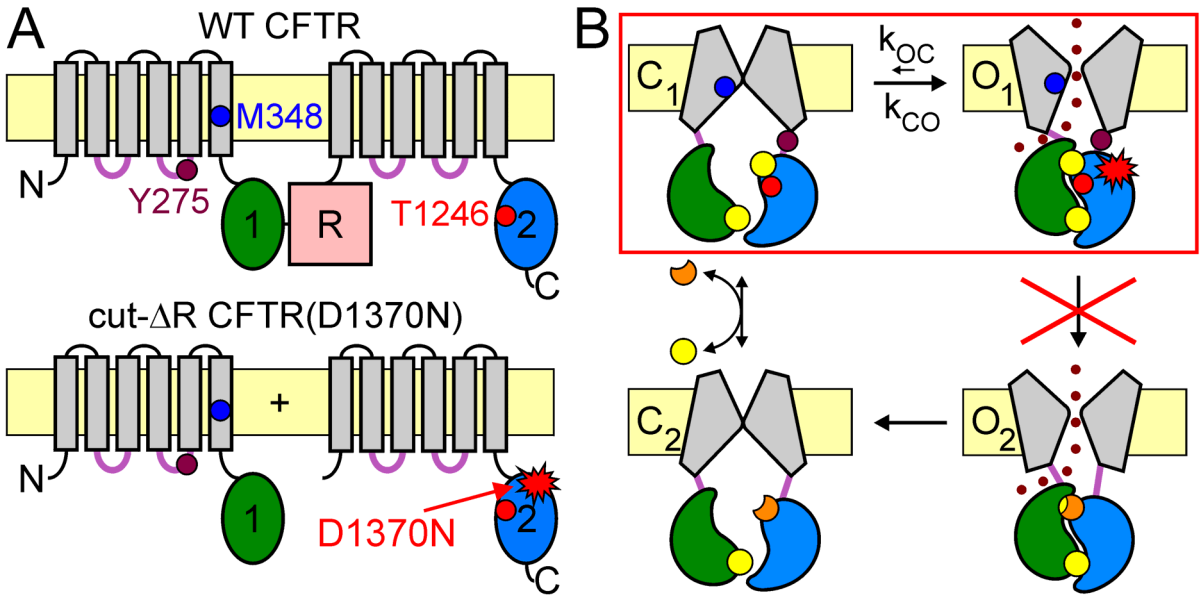
A
WT CFTR
M348
N
Y275
1
R
T1246
2
C
cut-ΔR CFTR(D1370N)
+
N
1
D1370N
2
C
B
C1
kOC
kCO
O1
C2
O2

Fig. 2

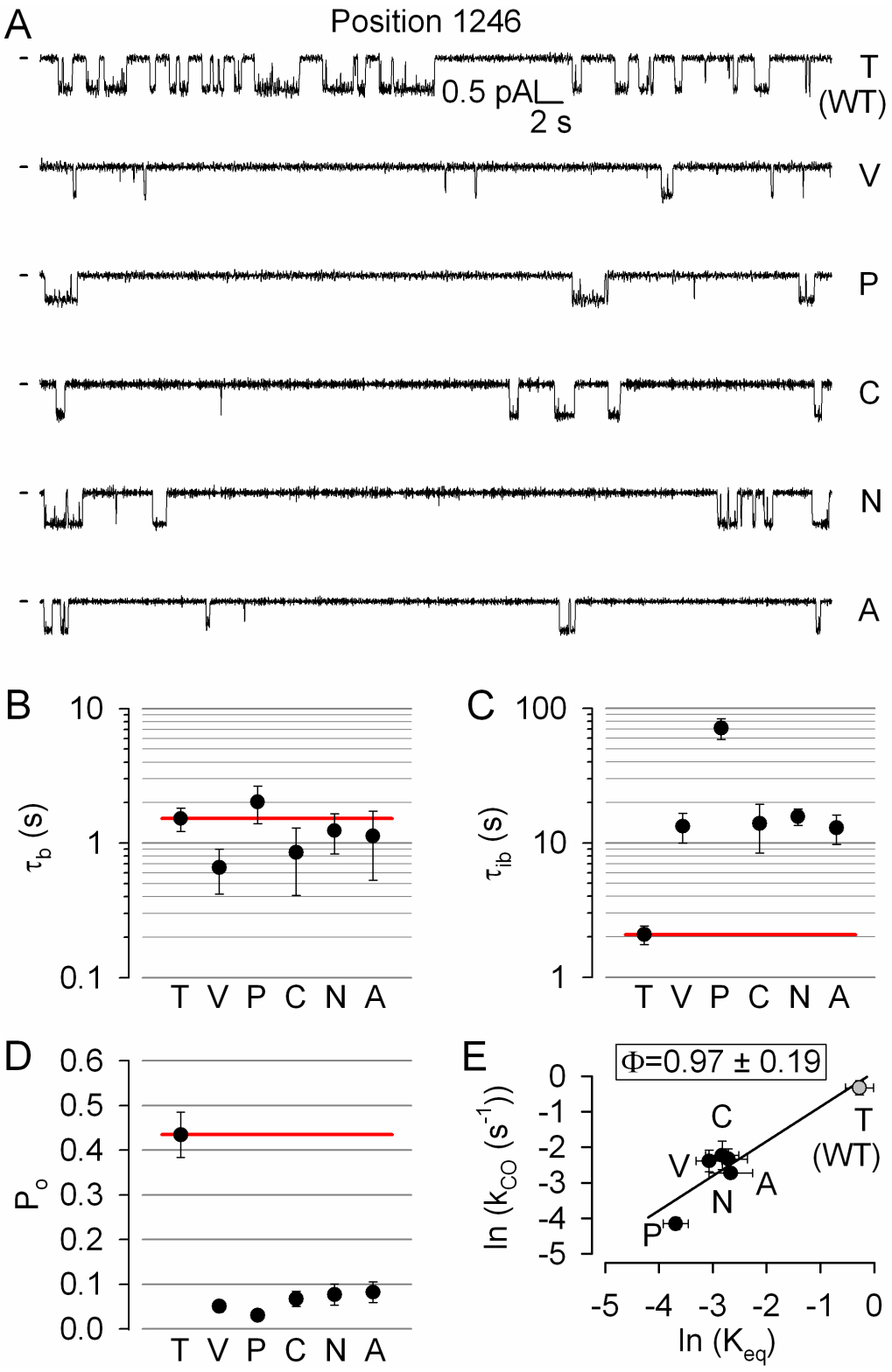
A
Position 1246
0.5 pA
2 s
T (WT)
V
P
C
N
A
B
10
1
0.1
τb (s)
T V P C N A
C
100
10
1
τib (s)
T V P C N A
D
0.6
0.5
0.4
0.3
0.2
0.1
0.0
Po
T V P C N A
E
Φ=0.97 ± 0.19
0
-1
-2
-3
-4
-5
ln (kCO (s-1))
C
T (WT)
V
A
N
P
-5 -4 -3 -2 -1 0
ln (Keq)

Fig. 3

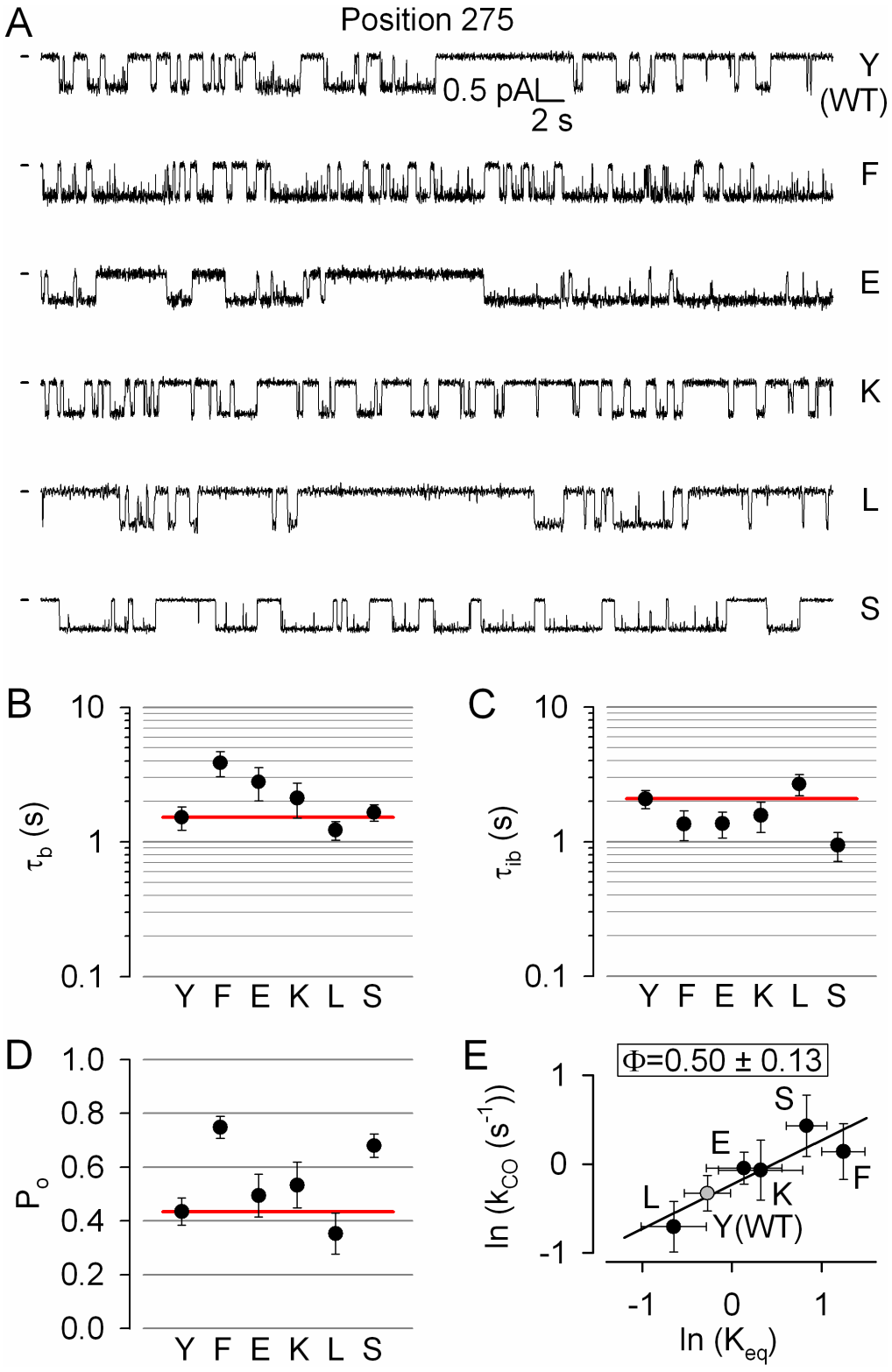
A
Position 275
0.5 pA
2 s
Y (WT)
F
E
K
L
S
B
10
1
0.1
τb (s)
Y F E K L S
C
10
1
0.1
τib (s)
Y F E K L S
D
1.0
0.8
0.6
0.4
0.2
0.0
Po
Y F E K L S
E
Φ=0.50 ± 0.13
1
0
-1
ln (kCO (s-1))
S
E
F
L
K
Y(WT)
-1
0
1
ln (Keq)

Fig. 4

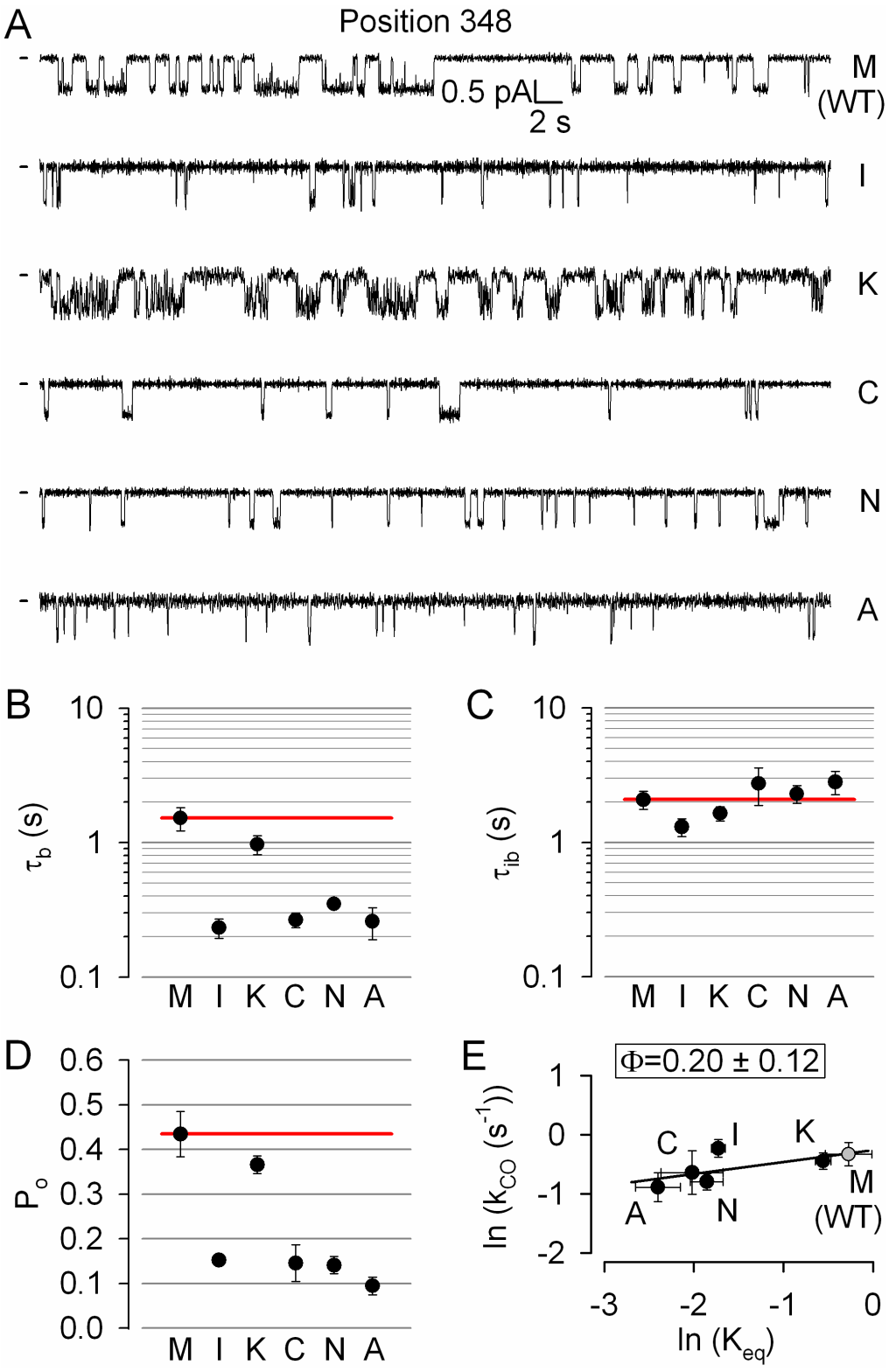
A
Position 348
0.5 pA
2 s
M (WT)
I
K
C
N
A
B
τ_b (s)
10
1
0.1
M I K C N A
C
τ_{ib} (s)
10
1
0.1
M I K C N A
D
P_o
0.6
0.5
0.4
0.3
0.2
0.1
0.0
M I K C N A
E
Φ=0.20 ± 0.12
ln (k_{CO} (s^{-1}))
1
0
-1
-2
C
I
K
A
N
M (WT)
-3
-2
-1
0
ln (K_{eq})

Fig. 5

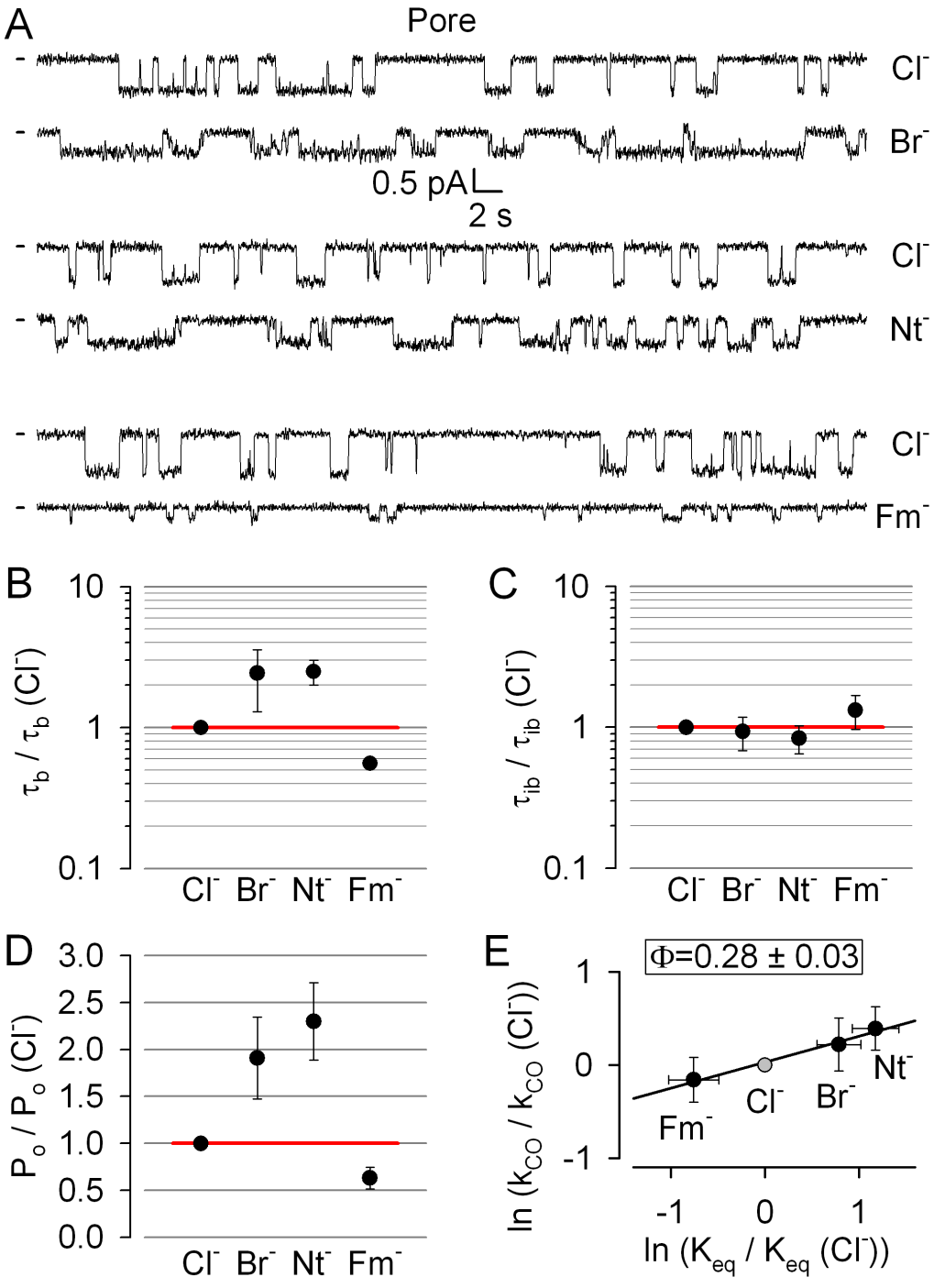
A
Pore
Cl-
Br-
0.5 pA
2 s
Cl-
Nt-
Cl-
Fm-
B
10
1
0.1
τb / τb (Cl-)
Cl- Br- Nt- Fm-
C
10
1
0.1
τib / τib (Cl-)
Cl- Br- Nt- Fm-
D
3.0
2.5
2.0
1.5
1.0
0.5
0.0
Po / Po (Cl-)
Cl- Br- Nt- Fm-
E
Φ=0.28 ± 0.03
1
0
-1
ln (kCO / kCO (Cl-))
Fm-
Cl-
Br-
Nt-
-1
0
1
ln (Keq / Keq (Cl-))

Fig. 6

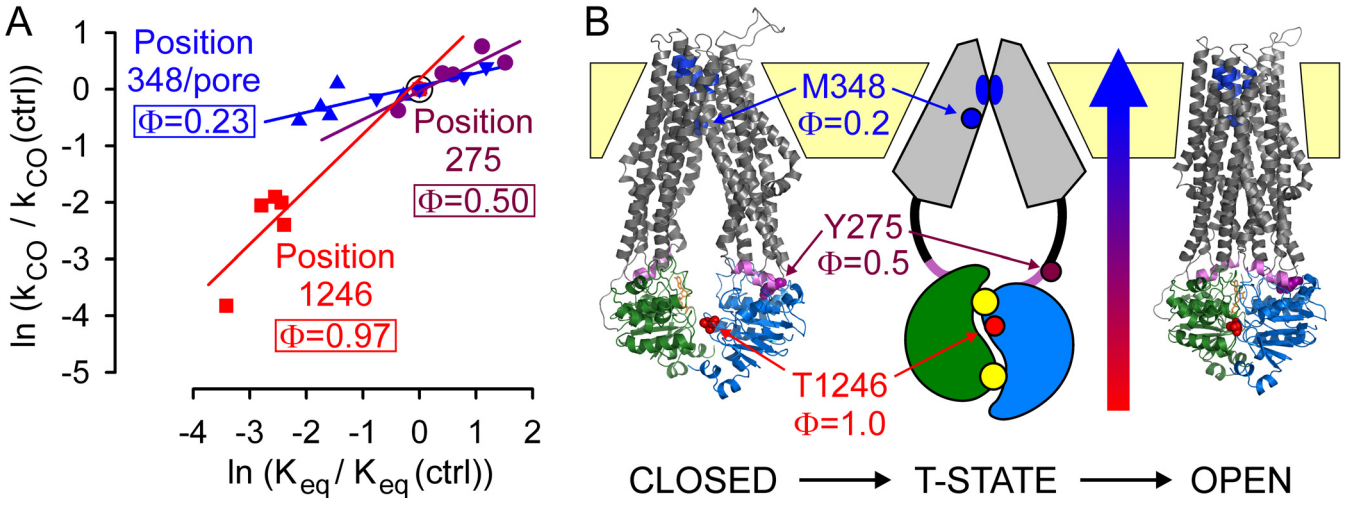
A
Position 348/pore
Φ=0.23
Position 275
Φ=0.50
Position 1246
Φ=0.97
ln (k_CO / k_CO (ctrl))
ln (K_eq / K_eq (ctrl))
1
0
-1
-2
-3
-4
-5
-4 -3 -2 -1 0 1 2
B
M348
Φ=0.2
Y275
Φ=0.5
T1246
Φ=1.0
CLOSED
T-STATE
OPEN

Supplementary Figure Legends

Figure S1. All tested constructs are saturated by 10 mM ATP, Related to Figures 1-4. *A*, Macroscopic inward cut-ΔR(D1370N) CFTR channel current in an inside-out patch recorded at -80 mV in response to exposures (*green bars*) to various concentrations (*green numbers*, in mM) of MgATP. *B*, Dose response curve of fractional macroscopic currents in various test [ATP], normalized to the mean of the currents in the presence of bracketing applications of 10 mM ATP. All data are shown as mean ± SEM (n = 5-10). Solid line is a Michaelis-Menten fit through the data with $K_{1/2}$ indicated. *C*, Fractional macroscopic currents in 3 mM ATP, normalized to the mean of the currents in the presence of bracketing applications of 10 mM ATP, for cut-ΔR(D1370N) channels harbouring the indicated amino-acid substitutions (*letters*) at position 1246 (*red bars*), 275 (*violet bars*), or 348 (*blue bars*). The larger than unity (*gray line*) value for M348K reflects pronounced block of this mutant by 10 mM ATP (see text). All data are shown as mean ± SEM (n = 3-8).

Figure S2. Time constants of macroscopic current relaxation following ATP removal corroborate steady-state single-channel estimates of τ_b, Related to Figures 1-5. *A*, *D-G*, Inward macroscopic currents of cut-ΔR(D1370N) CFTR (*A*), and of the same background construct harbouring mutation T1246A (*D*), Y275F (*E*), M348K (*F*), or M348E (*G*), elicited by exposure to 10 mM MgATP (*green bars*). *B-C*, Inward macroscopic currents of cut-ΔR(D1370N) CFTR evoked by repetitive exposures to 10 mM ATP in the alternating presence of various bath anions (*gray/light-blue bars*; chloride (Cl^-), bromide (Br^-), nitrate (Nt^-), formate (Fm^-)). All recordings were obtained at -80 mV; all current relaxation time courses following ATP removal in *A-G* were fitted by single exponentials (*colored solid lines*) with time constants (τ) indicated. *H*, Macroscopic current relaxation time constants upon ATP removal for the constructs/ionic conditions shown in *A-G*. All data are shown as mean ± SEM (n = 2-9), *gray line* highlights the control value for cut-ΔR(D1370N) CFTR in chloride.

Figure S3. Burst analysis of cut-ΔR(D1370N) single-channel recording, Related to Experimental Procedures. ***A*,** Inward current of a single cut-ΔR(D1370N) channel repetitively exposed to 10 mM MgATP (*green bars*). Upon readmission of ATP following prolonged exposure to an ATP-free solution channels sometimes reopen with a marked delay (*first asterisk*); infrequently channels also inactivate in the continued presence of ATP (*second asterisk*). Such inactive periods were identified by eye, and

excluded from our analysis. *B-C*, Closed (*B*) and open (*C*) dwell-time histograms (Sigworth and Sine, 1987) constructed from the events list of the record in *A*; lower binning limit is 12 ms. *Solid red lines* are maximum likelihood fits of the dwell-times by a double- and a single-exponential distribution, respectively, with time constants ($\tau_{(1, 2)}$) and fractional amplitudes (a_1, a_2) printed in the panels. *Dotted black lines* In panel *B* depict the two components of the fit; *vertical blue line* the burst delimiter (t_{crit}) calculated using the method of (Magleby and Pallotta, 1983): this method ensures unbiased estimation of mean burst and interburst durations by equalizing the probabilities of misassigning interburst events as flickery closures and vice versa. *D-E*, Dwell-time histograms of reconstructed interburst (*D*) and burst (*E*) events following suppression of closed events shorter than t_{crit}. *Solid red line* in *D* replots the longer component of the double-exponential fit in *A*: note, some flickery closures remain uncancelled (events above red fit line, right of blue line), but an equal number of interburst closures is cancelled (lack of events below red fit line, left of blue line). *Solid red line* in *E* is a maximum likelihood fit of the burst durations by a single-exponential distribution (τ, time constant).

Figure S4. Stimulation of open probability by 2'-deoxy-ATP facilitates counting channels for low-P_o T1246-position mutants, Related to Experimental Procedures. Inward current of a single cut-ΔR(D1370N) channel harbouring the T1246N mutation. After several minutes of low-P_o activity in 10 mM MgATP (*green bar*), exposure to 10 mM Mg-2'-deoxy-ATP robustly stimulated P_o. Lower panels progressively expand the time scale of indicated segments (*gray arrows*) of the panel above.

Supplementary References

Magleby, K.L. and Pallotta, B.S. (1983). Burst kinetics of single calcium-activated potassium channels in cultured rat muscle. J. Physiol *344*, 605-623.

Sigworth, F.J. and Sine, S.M. (1987). Data transformations for improved display and fitting of single-channel dwell time histograms. Biophys. J. *52*, 1047-1054.

Fig. S1

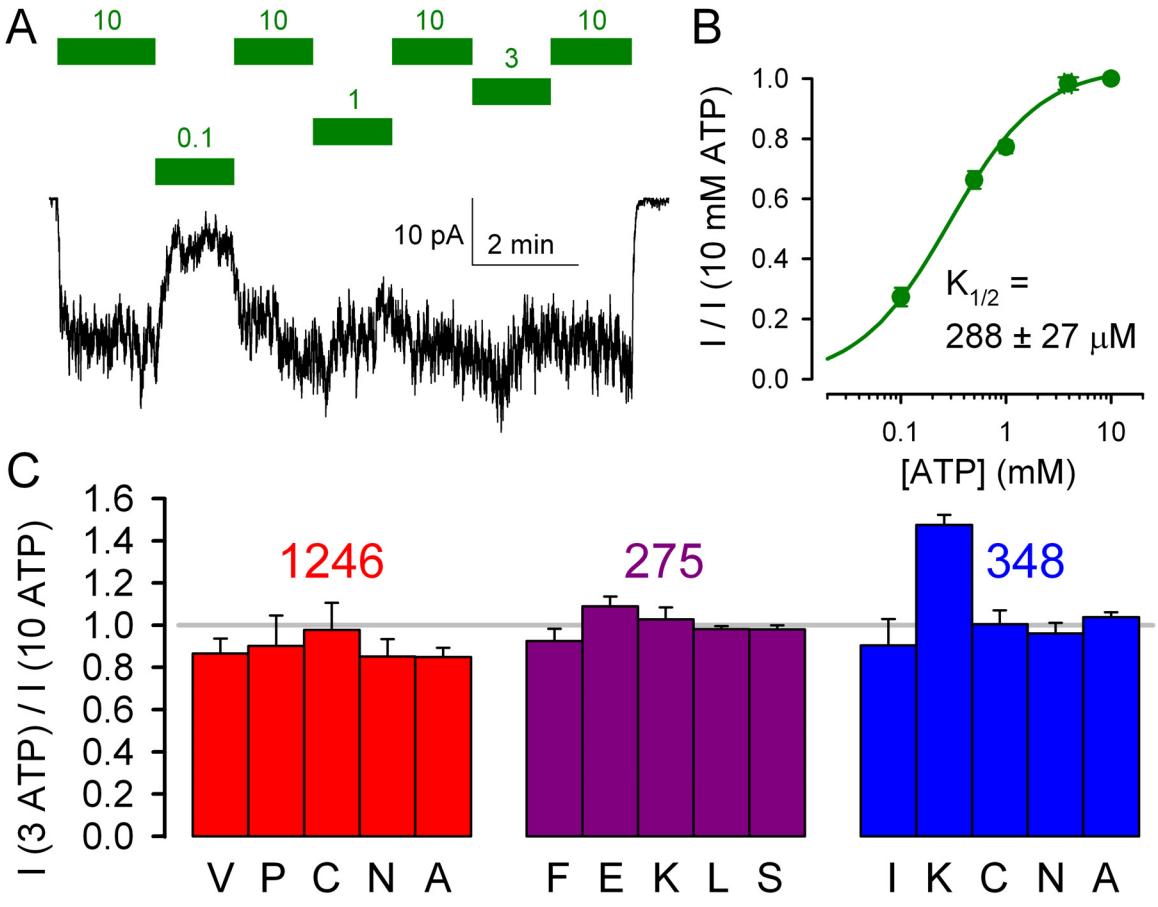
A
10
10
10
10
3
1
0.1
10 pA
2 min
B
I / I (10 mM ATP)
1.0
0.8
0.6
0.4
0.2
0.0
K1/2 =
288 ± 27 μM
0.1
1
10
[ATP] (mM)
C
I (3 ATP) / I (10 ATP)
1.6
1.4
1.2
1.0
0.8
0.6
0.4
0.2
0.0
1246
275
348
V P C N A
F E K L S
I K C N A

Fig. S2

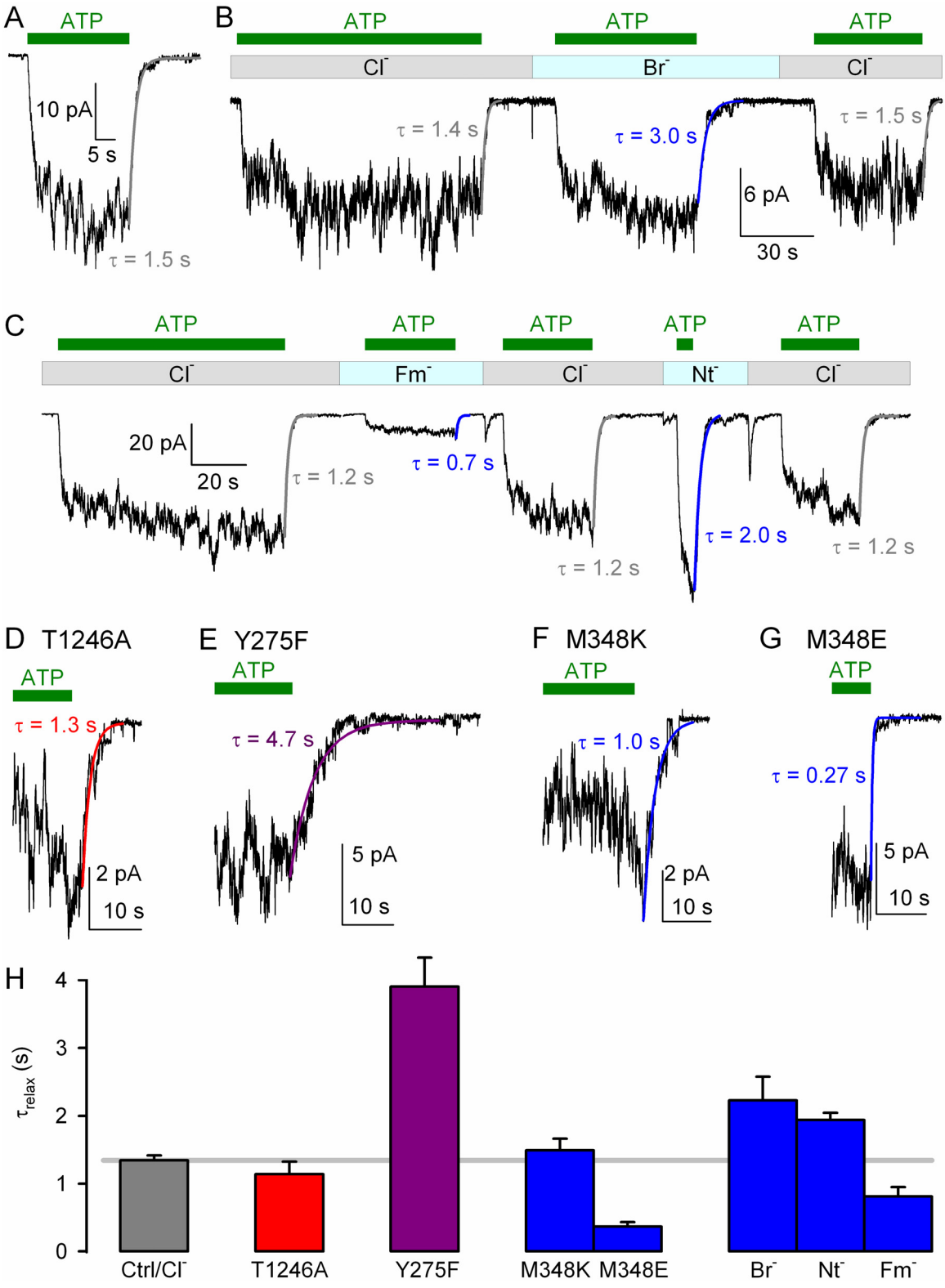
A
ATP
10 pA
5 s
τ = 1.5 s
B
ATP
ATP
ATP
Cl-
Br-
Cl-
τ = 1.4 s
τ = 3.0 s
τ = 1.5 s
6 pA
30 s
C
ATP
ATP
ATP
ATP
ATP
Cl-
Fm-
Cl-
Nt-
Cl-
20 pA
20 s
τ = 1.2 s
τ = 0.7 s
τ = 1.2 s
τ = 2.0 s
τ = 1.2 s
D T1246A
ATP
τ = 1.3 s
2 pA
10 s
E Y275F
ATP
τ = 4.7 s
5 pA
10 s
F M348K
ATP
τ = 1.0 s
2 pA
10 s
G M348E
ATP
τ = 0.27 s
5 pA
10 s
H
τrelax (s)
0
1
2
3
4
Ctrl/Cl-
T1246A
Y275F
M348K
M348E
Br-
Nt-
Fm-

Fig. S3

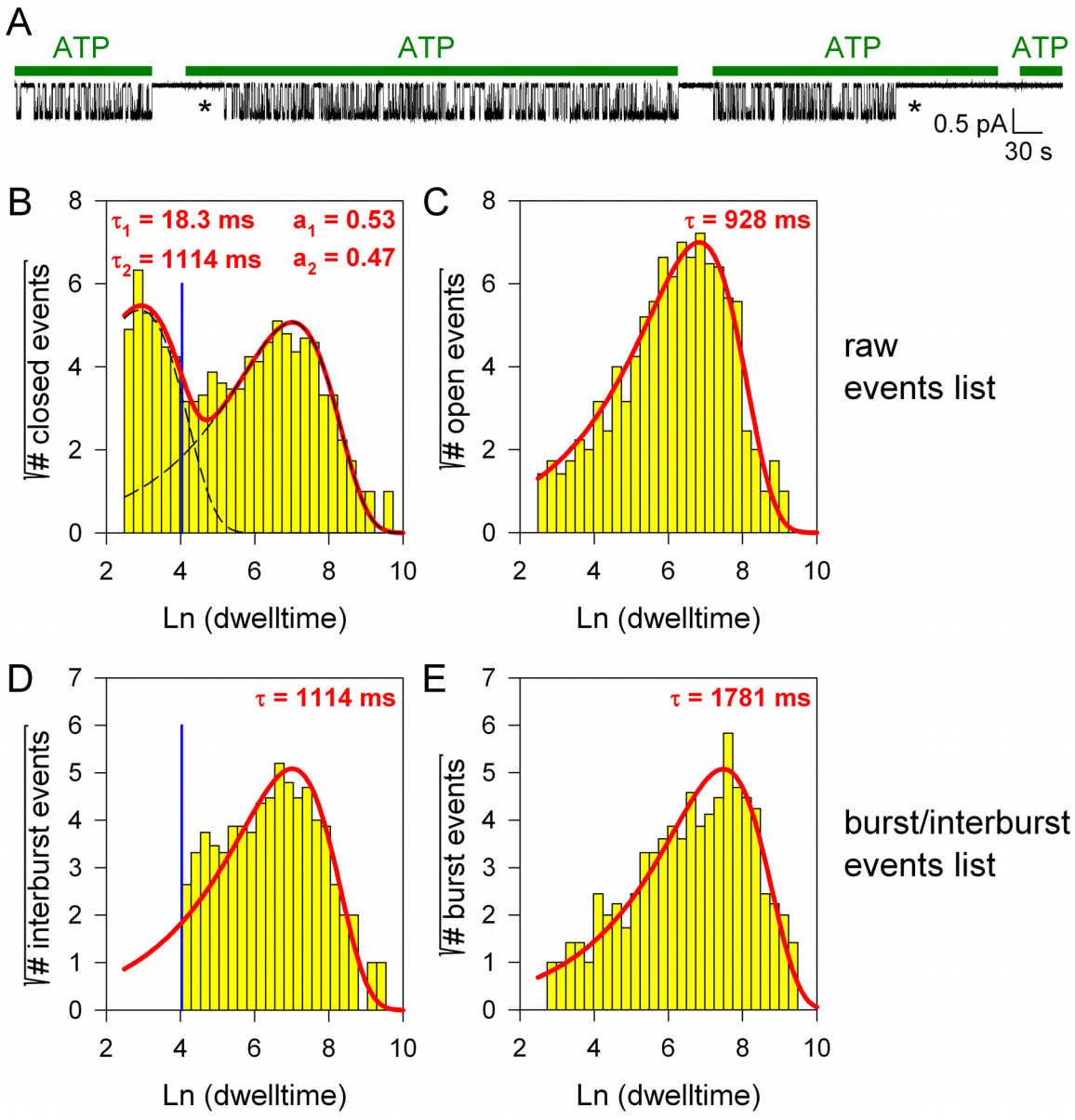
A
ATP
ATP
ATP
ATP
*
*
0.5 pA
30 s
B
τ1 = 18.3 ms
a1 = 0.53
τ2 = 1114 ms
a2 = 0.47
√# closed events
Ln (dwelltime)
C
τ = 928 ms
√# open events
Ln (dwelltime)
raw
events list
D
τ = 1114 ms
√# interburst events
Ln (dwelltime)
E
τ = 1781 ms
√# burst events
Ln (dwelltime)
burst/interburst
events list

Fig. S4